arXiv:cond-mat/0302007v1 [cond-mat.mes-hall] 1 Feb 2003

Exact time correlation functions for N classical Heisenberg spins in the 'squashed' equivalent neighbor model

Marco Ameduri[1, 2, *] and Richard A. Klemm[2, †]
[1] *Weill Cornell Medical College in Qatar, Qatar Foundation - Education City, P. O. Box 24144, Doha, Qatar*
[2] *Max-Planck-Institut für Physik komplexer Systeme,*
Nöthnitzer Straße 38, D-01187 Dresden, Germany

(Dated: February 2, 2008)

We present exact integral representations of the time-dependent spin-spin correlation functions for the classical Heisenberg N-spin 'squashed' equivalent neighbor model, in which one spin is coupled via the Heisenberg exchange interaction with strength J_1 to the other $N-1$ spins, each of which is coupled via the Heisenberg exchange interaction with strength J_2 to the remaining $N-2$ spins. At low temperature T we find that the N spins oscillate in four modes, one of which is a central peak for a semi-infinite range of the values of the exchange coupling ratio. For the $N=4$ case of four spins on a squashed tetrahedron, detailed numerical evaluations of these results are presented. As $T \to \infty$, we calculate exactly the long-time asymptotic behavior of the correlation functions for arbitrary N, and compare our results with those obtained for three spins on an isosceles triangle.

PACS numbers: 05.20.-y, 75.10.Hk, 75.75.+a, 05.45.-a

I. INTRODUCTION

Recently there has been a growing interest in the study of the properties of magnetic molecules. [1, 2, 3, 4, 5] The defining characteristic of these substances is the presence of a small cluster of magnetic ions located at the center of each molecule and surrounded by a complicated structure of non-magnetic chemical ligand groups. In general, the strength of the magnetic interaction between ions located in different molecules is negligible in comparison to the strength of their intramolecular interactions. Therefore, measurements of the magnetic properties of macroscopic samples reflect the underlying magnetic interactions within a single molecule.

The list of synthesized magnetic molecules has been constantly growing, even though most of the experimental activity has been focused on the determination of the magnetic properties of a molecule containing twelve manganese ions at its core, often referred to as Mn_{12}. The theoretical tools currently used to describe the behavior of this relatively complicated structure are still rudimentary, and are based on a single-spin phenomenological Hamiltonian. [1] It is important to notice that a number of molecular structures containing smaller numbers of magnetic ions have already been synthesized. For some of these structures it is possible to perform a more detailed theoretical analysis of their magnetic behavior starting from a many-spin Hamiltonian.

Among the smaller clusters are a regular tetrahedron of Cr^{3+} ions ($S=\frac{3}{2}$) [2, 3], Cr_4, and a squashed tetrahedron of Fe^{3+} ions ($S=\frac{5}{2}$) [4, 5], Fe_4. For increasing values of the spin a description in terms of classical spins is expected to capture many of the features of the system [6, 7]. In the present paper we provide exact expressions for the time-dependent spin-spin correlation functions for the classical Heisenberg N-spin squashed equivalent neighbor model, which is the N-spin generalization of four classical Heisenberg spins on the corners of a squashed tetrahedron. Specific numerical results for the squashed tetrahedron case, $N=4$, are provided. Analogous studies have recently appeared for three spins on an isosceles triangle and on a chain [8], for four spins on a square ring [9], and for the equivalent neighbor model of N classical spins [10]. Quantum time-dependent correlation functions have been computed for a dimer [6] and for three spins on an equilateral triangle [7], and for a dimer of classical and quantum spins in a constant magnetic field [11]. The availability of time-dependent correlation functions is necessary to analyze neutron scattering experiments.

In Section II we define the Hamiltonian system to be studied and write the corresponding partition function. In Section III we present the constraints upon the various correlation functions. In Section IV we present our analytic results for arbitrary N. We evaluate the long-time behavior of the correlation functions at infinite temperature T, and provide analytic formulae for the low-T modes for arbitrary N. In Section V, we present numerical results at low T for the squashed tetrahedron, $N=4$. Section VI contains our conclusions. A collection of intermediate steps useful to the calculations is compiled in the Appendix.

II. THE MODEL

We consider N classical spins of unit magnitude, $|\boldsymbol{S}_i|=1$, interacting according to the Hamiltonian

$$H=-\frac{J_2}{2}\sum_{\substack{i,j=1\\ i\neq j}}^{M}\boldsymbol{S}_i\cdot\boldsymbol{S}_j-J_1\boldsymbol{S}_N\cdot\sum_{i=1}^{M}\boldsymbol{S}_i, \tag{1}$$

where

$$M \equiv N - 1 \geq 2. \tag{2}$$

Introducing the total spin $\boldsymbol{S} = \sum_{i=1}^{N} \boldsymbol{S}_i$ and the auxiliary variable $\boldsymbol{S}_{1\to M} = \sum_{i=1}^{M} \boldsymbol{S}_i = \boldsymbol{S} - \boldsymbol{S}_N$, the Hamiltonian (1) can be written as

$$H = -\frac{J_1}{2}\boldsymbol{S}^2 - \frac{J_2 - J_1}{2}\boldsymbol{S}_{1\to M}^2, \tag{3}$$

where we have dropped the constant energy $(J_1 + MJ_2)/2$. The partition function can then be calculated following the technique described in [9, 12]. Letting $s = |\boldsymbol{S}|$ and $x = |\boldsymbol{S}_{1\to M}|$, one obtains

$$\begin{aligned} Z &= \int_0^M dx \mathcal{D}_M(x) \int_{|x-1|}^{x+1} s ds \exp(-\beta H) && (4) \\ &= \frac{e^{\alpha}}{\alpha} \int_0^M dx \mathcal{D}_M(x) \exp(\alpha\gamma x^2) \sinh(2\alpha x), && (5) \end{aligned}$$

where $\beta = (k_{\rm B}T)^{-1}$, $\alpha = \beta J_1/2$, $\gamma = J_2/J_1$, and $\mathcal{D}_M(x)$ is the classical M-spin density of states,[10] which we redisplayed in Eq. (A44) in the Appendix.

In order to compute the time-dependent correlation functions, we first solve the classical equations of motion appropriate for the Hamiltonian, Eq. (3),

$$\dot{\boldsymbol{S}}_{N,1\to M} = J_1 \boldsymbol{S}_{N,1\to M} \times \boldsymbol{S} \tag{6}$$

and $\dot{\boldsymbol{S}} = 0$, so that $\boldsymbol{S}$ is a constant of the motion. Following the technique illustrated in [8, 9, 10], we obtain

$$\begin{aligned} \boldsymbol{S}_{N,1\to M}(t) &= C_{N,1\to M}\hat{\boldsymbol{s}} + A_{N,1\to M} \\ &\quad \times \left[\cos(st^*)\hat{\boldsymbol{x}} - \sin(st^*)\hat{\boldsymbol{y}}\right], && (7) \end{aligned}$$

where $t^* = J_1 t$, $\hat{\boldsymbol{s}} = \boldsymbol{S}/s = \hat{\boldsymbol{x}} \times \hat{\boldsymbol{y}}$, $C_N = (s^2 - x^2 + 1)/(2s)$, $C_{1\to M} = (s^2 + x^2 - 1)/(2s)$, $A_N^2 = 1 - C_N^2$, and $A_N = -A_{1\to M}$.

We must also consider the equations of motion for the $\boldsymbol{S}_i(t)$, $i = 1, 2, \ldots, M$. In order to calculate the time correlation functions, symmetry allows us to choose just one of them, $i = 1$. We then write $\boldsymbol{S}_{1\to M} = \boldsymbol{S}_1 + \boldsymbol{S}_{2\to M}$, and solve

$$\dot{\boldsymbol{S}}_{1,2\to M} = J_2 \boldsymbol{S}_{1,2\to M} \times \boldsymbol{S} + (J_1 - J_2)\boldsymbol{S}_{1,2\to M} \times \boldsymbol{S}_N. \tag{8}$$

After defining $S_{1\pm} = S_{1x} \pm iS_{1y}$, we obtain,

$$\begin{aligned} S_{1\pm}(t) &= -\frac{A_N S_{1z0}}{C_{1\to M}} \exp(\mp ist^*) - \frac{A_N \Delta S_{1z0}}{2(C_{1\to M} \mp x)} \\ &\quad \times \exp\left\{i\left[\mp s + (1-\gamma)x\right]t^* + i\phi_0\right\} \\ &\quad -\frac{A_N \Delta S_{1z0}}{2(C_{1\to M} \pm x)} \\ &\quad \times \exp\left\{i\left[\mp s - (1-\gamma)x\right]t^* - i\phi_0\right\}, && (9) \\ S_{1z}(t) &= S_{1z0} + \Delta S_{1z0}\cos\left[(1-\gamma)xt^* + \phi_0\right], && (10) \end{aligned}$$

where ϕ_0 is an arbitrary phase, and similar equations for the components of $\boldsymbol{S}_{2\to M}$. After combining these equations with analogous ones for the components of $\boldsymbol{S}_{1\to M}$, the constants appearing in Eqs. (9) and (10) must satisfy

$$\begin{aligned} S_{1z0} &= \frac{C_{1\to M}}{2}\left(1 + \frac{1-y^2}{x^2}\right), && (11) \\ (\Delta S_{1z0})^2 &= \frac{A_{1\to M}^2}{x^2}\left[1 - \frac{(x^2 - y^2 + 1)^2}{4x^2}\right], && (12) \end{aligned}$$

where $y = |\boldsymbol{S}_{2\to M}|$.

Previously, we solved these equations for the simplest case, $M = 2$, for which $y = 1$ is not a variable.[8] In that case, the correlation functions were obtained from the double integrals over x and s, according to the weighting factors in Eq. (4). For $M \geq 3$, however, y can vary over the entire range $0 \leq y \leq M - 1$. Hence, for the explicit evaluation of the correlation functions with $M \geq 3$, it is useful to rewrite the expression of the partition function (4) in terms of a triple integral over s, x, and y,

$$Z = \int_0^{M-1} \mathcal{D}_{M-1}(y) dy \int_{|y-1|}^{y+1} dx \int_{|x-1|}^{x+1} s ds \exp(-\beta H). \tag{13}$$

III. CONSTRAINTS

In this section we analyze the constraints upon the time-dependent spin-spin correlation functions

$$\mathcal{C}_{ij}(t) = \langle \boldsymbol{S}_i(t) \cdot \boldsymbol{S}_j(0) \rangle, \tag{14}$$

where the thermal average $\langle \ldots \rangle$ is performed by averaging over the arbitrary phase ϕ_0 and the variables s, x, and y, with respect to the canonical ensemble defined by Eq. (13). Due to the symmetry of the molecule, only four of the $N(N+1)/2$ correlation functions in Eq. (14) are distinct. We write these as $\mathcal{C}_{11}(t)$, $\mathcal{C}_{12}(t)$, $\mathcal{C}_{1N}(t)$, and $\mathcal{C}_{NN}(t)$. Conservation of the total spin adds a constraint,

$$\begin{aligned} \langle s^2 \rangle &= \mathcal{C}_{NN}(t) + M\mathcal{C}_{11}(t) + 2M\mathcal{C}_{1N}(t) \\ &\quad + M(M-1)\mathcal{C}_{12}(t). && (15) \end{aligned}$$

Finally, by writing the multispin correlation function $\langle \boldsymbol{S}_{1\to M}(t) \cdot \boldsymbol{S}_{1\to M}(0) \rangle$ in two ways, we find a second constraint between two of the correlation functions,

$$\langle sC_N \rangle = \mathcal{C}_{NN}(t) + M\mathcal{C}_{1N}(t), \tag{16}$$

where the constant C_N is given just below Eq. (7). The two remaining independent correlation functions $\mathcal{C}_{NN}(t)$ and $\mathcal{C}_{11}(t)$ must then be calculated by explicitly substituting into Eq. (14) the time dependences obtained in Section II. For $\mathcal{C}_{NN}(t)$, this is relatively simple, as one can just use Eq. (7) for $\boldsymbol{S}_N(t)$, which is independent of y, to evaluate it. This leads to

$$\mathcal{C}_{NN}(t) = \langle C_N^2 + A_N^2 \cos(st^*) \rangle, \tag{17}$$

which can be evaluated using the simplified weighting factors present in Eq. (4). From Eq. (16), this simplification also applies for $\mathcal{C}_{1N}(t)$. We note that Eq. (17) differs from the expression for the autocorrelation function in the N-spin classical Heisenberg equivalent neighbor model only by the x dependence of the Hamiltonian,[10] which is irrelevant as $T \to \infty$.

The challenge is to calculate $\mathcal{C}_{11}(t)$. It is useful to separate the expression for $\mathcal{C}_{11}(t)$ into the four integrals $I_i(t)$ $(i = 0, \ldots, 3)$,

$$\mathcal{C}_{11}(t) = \sum_{i=0}^{3} I_i(t). \tag{18}$$

The explicit triple integral representations of the $I_i(t)$ valid for arbitrary T are given in the Appendix, where it is also shown how to reduce them to double integrals.

IV. ANALYTIC RESULTS FOR ARBITRARY N

A. Infinite temperature limit

Here we present our results for the correlation functions with general N values as $T \to \infty$. As shown in the Appendix, in the limit $T \to \infty$, the triple integrals appearing in (18) can be reduced to single integrals. For $N = 4$, the relevant density of states appearing in Eq. (13) is $\mathcal{D}_2(x) = \frac{1}{2}\Theta(x)\Theta(2-x)$, so this reduction in the number of integrals is relatively simple. As $T \to \infty$, the different couplings appearing in the Hamiltonian become irrelevant for $\mathcal{C}_{NN}(t)$, so that it becomes equivalent to that of the N-spin equivalent-neighbor model,[10]

$$\lim_{T\to\infty} \mathcal{C}_{NN}(t) = 1/N + M[\delta_N + f_N(t)], \tag{19}$$

where $f_N(t) \sim (t^*)^{-N}$ for $t^* \gg 1$. Since as $T \to \infty$, $\langle s^2\rangle = N$, $\langle x^2\rangle = M$, and $\langle y^2\rangle = M - 1$, from Eqs. (16) and (19), we have

$$\lim_{T\to\infty} \mathcal{C}_{1N}(t) \;=\; 1/N - \delta_N - f_N(t). \tag{20}$$

For $\mathcal{C}_{11}(t)$ and $\mathcal{C}_{12}(t)$, even as $T \to \infty$, the situation is more complicated, as the results depend crucially upon the values of $\gamma = J_2/J_1$. As $t \to \infty$, the time-dependent trigonometric functions in I_1, I_2, and I_3 oscillate increasingly rapidly and yield vanishing contributions to $\lim_{t\to\infty} \mathcal{C}_{11}(t)$, as stated by the Riemann-Lebesgue lemma [13]. Therefore, for arbitrary N,

$$\lim_{t\to\infty} \mathcal{C}_{11}^{\gamma\neq 1}(t) = I_0 = \langle S_{1z0}^2\rangle, \tag{21}$$

We note that I_0 depends upon N, and is a rather messy triple integral, but that as $T \to \infty$, can be evaluated exactly, as shown in the Appendix.

At infinite temperature one obtains for $N = 4$,

$$\lim_{\substack{t\to\infty\\ T\to\infty}} \mathcal{C}_{44}(t) = \frac{1}{4} + 3\delta_4 \approx 0.436345, \tag{22}$$

where $\delta_4 = -(11/180) + (8/45)\ln 2 \approx 0.062115$, [9, 10] and

$$\lim_{\substack{t\to\infty\\ T\to\infty}} \mathcal{C}_{11}^{\gamma\neq 1}(t) \;\approx\; 0.355496, \tag{23}$$

the exact expression for which is given in (A47) in the Appendix. In Table I in the Appendix, we also list the $T \to \infty$ values of $\lim_{t\to\infty} \mathcal{C}_{11}^{\gamma\neq 1}(t)$ for $3 \le N \le 11$, and compare them with the $T \to \infty$ values of $\lim_{t\to\infty} \mathcal{C}_{NN}(t)$. We note that as $T \to \infty$, for each of these N values, $\lim_{t\to\infty} \mathcal{C}_{11}^{\gamma\neq 1}(t) < \lim_{t\to\infty} \mathcal{C}_{NN}(t)$. As $T \to \infty$, $\lim_{t\to\infty} \mathcal{C}_{NN}(t)$ decreases monotonically with increasing N to $\frac{1}{3}$ as $N \to \infty$.[10] Since $\lim_{t\to\infty} \mathcal{C}_{11}^{\gamma\neq 1}(t)$ also decreases monotonically with increasing N, and for $8 \le N \le 11$, its value is less than $\frac{1}{3}$, it appears that this inequality is likely to hold for all N values.

We now turn to the long-time asymptotic behavior of $\mathcal{C}_{11}(t)$ at infinite T. Following the method described in [8], we first define $\delta\mathcal{C}_{ij}(t) \equiv \mathcal{C}_{ij}(t) - \lim_{t\to\infty} \mathcal{C}_{ij}(t)$. For $\gamma = 0$, the dominant behavior of $\lim_{T\to\infty} \mathcal{C}_{11}(t)$ is given by $I_3(t)$, but for $0 \neq \gamma \neq 1$, it is given by $I_2(t)$. At long times, $\overline{t} \gg 1$, where $\overline{t} = (1-\gamma)t^*$, one can evaluate the asymptotic behavior as $T \to \infty$ exactly. By integration by parts M times, we find,

$$\lim_{\substack{T\to\infty\\ \overline{t}\gg 1}} \delta\mathcal{C}_{11}^{\gamma\neq 0,1}(t) \;\sim\; \sum_{p=0}^{E(M/2)} \frac{A_{Mp}}{(\overline{t})^M} f(M-2p) \times\cos[(M-2p)\overline{t} + M\pi/2], \tag{24}$$

where

$$f(y) \;=\; 1 + y^{-2} - \frac{(y^2-1)^2}{4y^3}\ln\Bigl(\frac{y+1}{y-1}\Bigr)^2 \tag{25}$$

and A_{Mp} is given in the Appendix. Although the function $f(y)$ is non-analytic at $y = 1$, it can be shown that its derivatives do not contribute to the long-time asymptotic behavior. In addition, for $t^* \gg 1$, one can easily obtain the asymptotic expression of $I_3(t)$, leading to

$$\lim_{\substack{T\to\infty\\ t^*\gg 1}} \delta\mathcal{C}_{11}^{\gamma=0}(t) \;\sim\; \frac{\sin(t^*)}{4t^*}\int_0^{M-1} dy\mathcal{D}_{M-1}(y) \times y^3 f(y). \tag{26}$$

In particular, for $N = 4$, we obtain

$$\lim_{\substack{T\to\infty\\ t^*\gg 1}} \delta\mathcal{C}_{44}(t) \;\sim\; -\frac{3}{4(t^*)^4}\left[\frac{3}{4} - \cos(4t^*)\right], \tag{27}$$

$$\lim_{\substack{T\to\infty\\ \overline{t}\gg 1}} \delta\mathcal{C}_{11}^{\gamma\neq 0,1}(t) \;\sim\; -\frac{1}{8(\overline{t})^3}\Bigl[f(1)\sin(\overline{t}) + f(3)\sin(3\overline{t})\Bigr], \tag{28}$$

$$\lim_{\substack{T\to\infty\\ t^*\gg 1}} \delta\mathcal{C}_{11}^{\gamma=0}(t) \;\sim\; \left(\frac{23}{30} - \frac{9}{40}\ln 3\right)\frac{\sin(t^*)}{t^*}, \tag{29}$$

where Eq. (27) was given previously.[9, 10]

It is interesting to compare the present results to the analogous ones obtained for the isosceles triangle of spins, $N = 3$. [8] For $N \geq 4$, the infinite-T, long-time behavior of $\mathcal{C}_{11}(t)$ for $\gamma \neq 0, 1$ is determined by the integral $I_2(t)$ given by Eq. (A41). For $N = 3$, an additional contribution to the infinite-T, long-time behavior of $\mathcal{C}_{11}(t)$ arises from $I_3(t)$ given by Eq. (A42). [8] For $N \geq 3$, the correlation function $\mathcal{C}_{11}(t)$ for $\gamma \neq 0, 1$ decays slower than $\mathcal{C}_{NN}(t)$ [denoted $\mathcal{C}_{22}(t)$ in Ref. [8] for $N = 3$], approaching its long-time asymptotic value at infinite temperature as $(t^*)^{-M}$. In the limiting situation $\gamma = 0$, corresponding for $N = 3$ to the three-spin chain (or 'two-pronged star') and for $N \geq 4$ to an M-pronged star of spins equally coupled to a central one, as $T \to \infty$ and $t^* \gg 1$, the correlation function is dominated by $I_3(t)$. In this case, $\mathcal{C}_{11}(t)$ approaches its asymptotic limit much more slowly, as $(t^*)^{-1}$, as shown in Eq. (26).

B. Low-temperature correlation functions

At any finite temperature, it is not possible to reduce the time-dependent correlation functions to a single integral representation, even for $N = 4$. Since the time-dependence of the integrand is a simple trigonometric function, it is convenient to compute the Fourier transforms of the $\delta\mathcal{C}_{ij}(t)$, quantities which are anyhow of direct experimental relevance in neutron scattering experiments. In this case, it is then possible to express the Fourier transforms in terms of a single integral representation, which then allows a precise and fast numerical integration. We limit our numerical work to the case of the squashed tetrahedron, $N = 4$ ($M = 3$).

We define the Fourier transform as usual as

$$\delta\tilde{\mathcal{C}}_{ij}(\omega) = \frac{|J_1|}{\pi}\int_{-\infty}^{+\infty} dt \exp(i\omega t)\delta\mathcal{C}_{ij}(t). \tag{30}$$

The position of the various peaks as a function of γ may be obtained analytically in the $T \to \infty$ limit through an asymptotic evaluation of the integrals, or numerically by plotting the curves at large enough values of $|\alpha| \propto 1/T$. In the Appendix, we have sketched the derivation of the low-temperature mode frequencies for general N, for both FM and AFM cases. For ferromagnetic couplings, we then find,

$$\Omega_1(\gamma)/J_1 = \begin{cases} M+1 & \text{for } \gamma \geq -1/M \\ 1 - 1/\gamma & \text{for } \gamma < -1/M \end{cases} \tag{31}$$

$$\Omega_2(\gamma)/J_1 = \begin{cases} 1 + M\gamma & \text{for } \gamma \geq -1/M \\ 0 & \text{for } \gamma < -1/M \end{cases} \tag{32}$$

$$\Omega_3(\gamma)/J_1 = \begin{cases} M|1-\gamma| & \text{for } 1 \neq \gamma \geq -1/M \\ 1 - 1/\gamma & \text{for } \gamma < -1/M \end{cases} \tag{33}$$

$$\Omega_4(\gamma)/J_1 = \begin{cases} |M(2-\gamma)+1| & \text{for } \gamma \geq -1/M \\ 2\,(1 - 1/\gamma) & \text{for } \gamma < -1/M, \end{cases} \tag{34}$$

and for antiferromagnetic couplings, we find,

$$\Omega_1(\gamma)/|J_1| = \begin{cases} |1 - 1/\gamma| & \text{for } \gamma \geq 1/M \\ M - 1 & \text{for } \gamma < 1/M \end{cases} \tag{35}$$

$$\Omega_2(\gamma)/|J_1| = \begin{cases} 0 & \text{for } \gamma \geq 1/M \\ 1 - M\gamma & \text{for } \gamma < 1/M \end{cases} \tag{36}$$

$$\Omega_3(\gamma)/|J_1| = \begin{cases} |1 - 1/\gamma| & \text{for } \gamma \geq 1/M \\ M(1-\gamma) & \text{for } \gamma < 1/M \end{cases} \tag{37}$$

$$\Omega_4(\gamma)/|J_1| = \begin{cases} 2\,|1 - 1/\gamma| & \text{for } \gamma \geq 1/M \\ M(2-\gamma) - 1 & \text{for } \gamma < 1/M. \end{cases} \tag{38}$$

We remark that these formulae also apply for the isosceles triangle, $M = 2$.[8]

V. LOW TEMPERATURE NUMERICAL RESULTS FOR $N = 4$

In Fig. 1, we plot the mode frequencies $\Omega_i(\gamma)$ relative to $|J_1|$, for the squashed tetrahedron case $M = 3$. The upper and lower panels correspond to the FM and AFM cases, respectively. The circle in the upper panel of Fig. 1 denotes the absence of a zero-frequency peak at all temperatures for the regular tetrahedron. We have verified these mode frequencies by numerical evaluation of the explicit integral representations of $\delta\tilde{\mathcal{C}}_{11}(\omega)$ and $\delta\tilde{\mathcal{C}}_{44}(\omega)$. For example, in Fig. 2 we show the low-T behavior of $\delta\tilde{\mathcal{C}}_{11}(\omega)$, presented as $\log_{10}[\delta\tilde{\mathcal{C}}_{11}(\omega)]$ versus $\omega/|J_1|$. For the FM case with $\gamma = 0.3$ at $\alpha = 50$ pictured in the upper panel of Fig. 2, $\delta\tilde{\mathcal{C}}_{11}(\omega)$ exhibits very sharp peaks at the frequencies Ω_i, where $\Omega_i/J_1 = 4, 1.9, 2.1$, and 6.1 for $i = 1, \ldots, 4$, respectively. $\delta\tilde{\mathcal{C}}_{44}(\omega)$ has a single sharp mode at the frequency Ω_1. This figure also shows that for $\gamma = 0.6$, the FM $\delta\tilde{\mathcal{C}}_{11}(\omega)$ modes are also sharp at $\alpha = 50$, appearing at 4, 2.8, 1.2, and 5.2, respectively, and at $\gamma = 0.9$, they appear at 4, 3.7, 0.3, and 4.3, respectively. We note that the Ω_4 mode is much weaker in intensity than the other modes at this temperature. For the AFM case, the modes tend to be much broader, as pictured for $\gamma = 0.6$ in the bottom panel of Fig. 2. In this case, the low-T mode frequencies satisfy $\Omega_i/|J_1| = 2/3, 0, 2/3, 4/3$, so that Ω_1 and Ω_3 are degenerate. This degeneracy is evident in the shape of the combined mode, which appears to consist of two peaks with different widths, both centered at $\omega/|J_1| = 2/3$. In addition, Ω_2 is a central peak, which grows in intensity as T decreases.

For the special case of the three-pronged star, $\gamma = 0$, the leading behaviors of the low-T modes are presented in Fig. 3. For the FM star, pictured in the upper panel of Fig. 3, we have plotted $n^2\delta\tilde{\mathcal{C}}_{ii}(\omega)$ versus $|\alpha|(\omega/J_1 - n)/n$ for the largest amplitude modes Ω_1 and Ω_2, for $i = 1, 4$. Since Ω_1 and Ω_2 appear at $\omega/J_1 = 4, 1$, respectively, and since the Ω_1 modes present in $\delta\tilde{\mathcal{C}}_{44}$ and $\delta\tilde{\mathcal{C}}_{11}$ are weaker

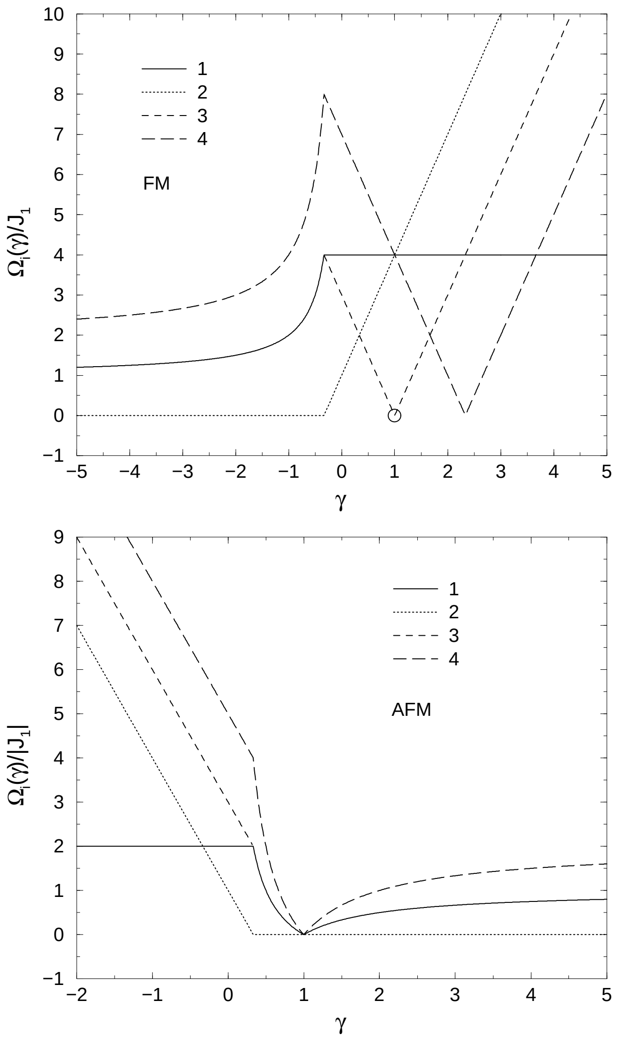

FIG. 1: The low-T magnon mode frequencies for the FM (top) and AFM (bottom) cases for the squashed tetrahedron ($M = 3$).

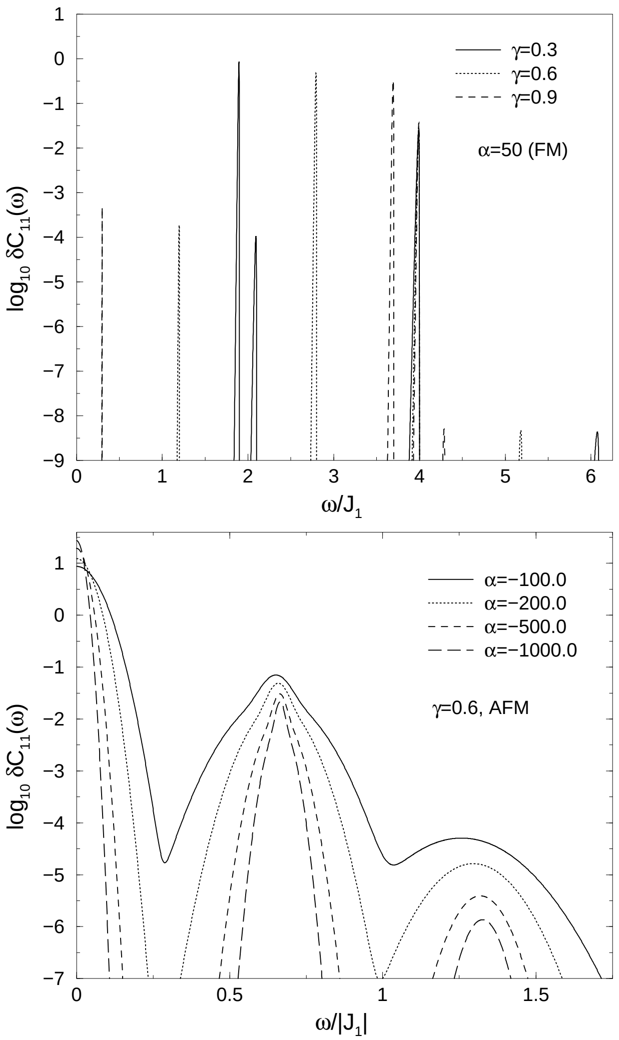

FIG. 2: Plots of $\log_{10}[\delta\tilde{\mathcal{C}}_{11}(\omega)]$ versus $\omega/|J_1|$ for the squashed tetrahedron ($M = 3$) at very low T. Top: FM case at $\alpha = 50$ for $\gamma = 0.3, 0.6, 0.9$. Bottom: AFM case for $\gamma = 0.6$ at various low T values.

than the Ω_2 mode, this presentation was chosen for clarity. Each of these modes was plotted at $\alpha = 5, 10$, and 20, demonstrating the low-T scaling that occurs. We also note that the Ω_2 mode in $\delta\tilde{\mathcal{C}}_{11}(\omega)$ drops discontinuously by many orders of magnitude (and to zero as $T \to 0$) at $\omega/J_1 = 1$, as indicated by the $\approx$ sign. This behavior is very similar to that of the FM chain, except for the difference in the frequencies involved.[8]

The AFM three-pronged star has parameters close to those present in the squashed tetrahedron Fe$_4$.[4, 5] The strongest low-T modes are pictured in the bottom panel of Fig. 3, in which we plotted $\delta\tilde{\mathcal{C}}_{ii}(\omega)$ versus $|\alpha|(\omega/|J_1| - n)/n$ for $i = 1, 4$, $n = 1, 2$, and $\alpha = -5, -10, -20$, and -40. Since these modes are sufficiently close in magnitude, the $\delta\tilde{\mathcal{C}}_{ii}(\omega)$ are not scaled in this figure. The additional modes at $\omega/|J_1| = 3, 5$ are very weak, and are not shown. As for the FM case, Ω_2 drops discontinuously by orders of magnitude at $\omega/|J_1| = 1$, vanishing as $T \to 0$. In addition, in both cases, the mode shapes approach uniform functions of $|\alpha|(\omega/|J_1| - n)$ as $T \to 0$. This behavior is actually simpler than that obtained for the AFM chain,[8] because in that case, the Ω_1 and Ω_2 modes present in $\delta\tilde{\mathcal{C}}_{11}(\omega)$ both approach the same frequency, $\omega/|J_1| = 1$, as $T \to 0$, making it difficult to separate them.

It is interesting to compare these findings with the simpler results in the case of a perfect tetrahedron (the equivalent neighbor model with $N = 4$. [10] There only one low-T mode is present, at $\Omega/J = 4$ in the ferromagnetic case, or at $\Omega = 0$ in the antiferromagnetic case. The low-T scaling of these single modes was shown previously.[10] Allowing one spin to be coupled differently induces a splitting in the spectrum of low-T magnons, a phenomenon which was already observed in the study of the isosceles triangle of spins. [8]

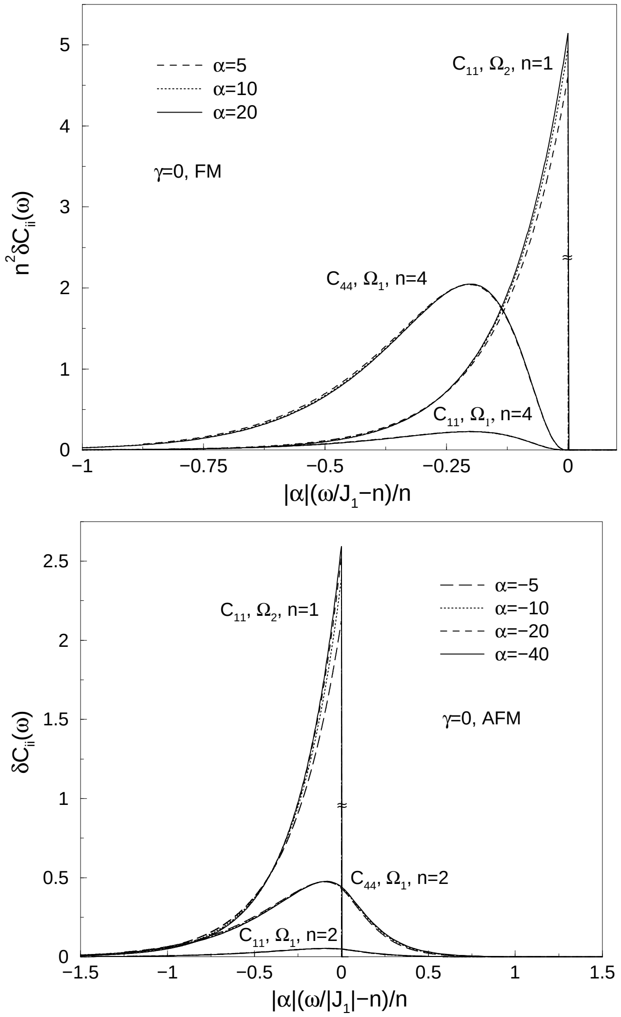

FIG. 3: Top: Plots for $M = 3$ of the Ω_1 and Ω_2 modes in $n^2\delta\tilde{\mathcal{C}}_{ii}(\omega)$ versus $|\alpha|(\omega/J_1 - n)/n$ with $i, n = 1, 4$ for the FM star, $\gamma = 0$, at $\alpha = 5, 10, 20$. Bottom: Plots for $M = 3$ of the Ω_1 and Ω_2 modes in $\delta\tilde{\mathcal{C}}_{ii}(\omega)$ versus $|\alpha|(\omega/|J_1| - n)/n$ with $i = 1, 4$ and $n = 1, 2$, for the AFM star, $\gamma = 0$, at $\alpha = -5, -10, -20$, and -40.

In Fig. 4, we plot the full temperature dependence of the two primary modes present for the AFM case with $\gamma = -0.05$, which is thought to be a better approximation to the parameters present in Fe$_4$ than in the bottom panel of Fig. 3. [4, 5] In this figure, we show the results of calculations for both $\delta\tilde{\mathcal{C}}_{11}(\omega)$ and $\delta\tilde{\mathcal{C}}_{44}(\omega)$ at $\alpha = 0, -1, -5$, and -20. At infinite T, $\alpha = 0$, $\delta\tilde{\mathcal{C}}_{44}(\omega)$ exhibits a broad peak with a maximum at $\omega/|J_1| \approx 1.7$, and $\delta\tilde{\mathcal{C}}_{11}(\omega)$ has substantial weight at low frequencies, a well-defined peak at $\omega/|J_1| \approx 0.8$, and a small peak at $\omega/|J_1| \approx 1.05$. As T is lowered, the peak in $\delta\tilde{\mathcal{C}}_{44}(\omega)$ develops into the sharp Ω_1 mode, approaching $\omega/|J_1| = 2$ as $T \to 0$. In addition, $\delta\tilde{\mathcal{C}}_{11}(\omega)$ develops into the two modes Ω_2 and Ω_1 at $\omega/|J_1| = 1.05$ and 2, respectively. The minor peaks at $\omega/|J_1| \approx 3.15$ and 5.15 are too weak to show up on the scale used in this figure.

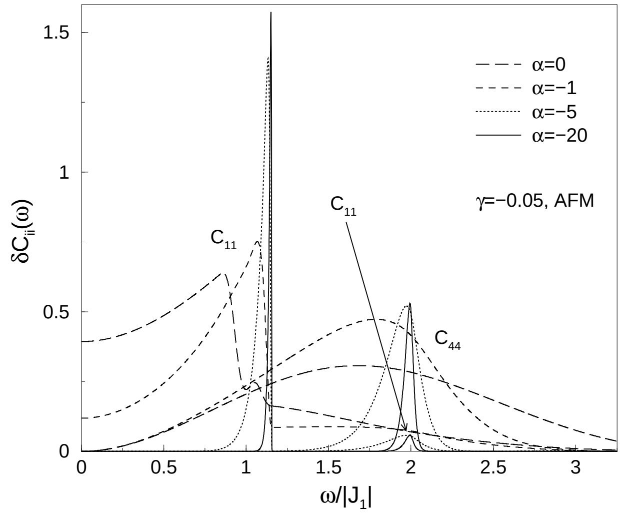

FIG. 4: Plots for $M = 3$ of $\delta\tilde{\mathcal{C}}_{ii}(\omega)$ versus $\omega/|J_1|$ at various temperatures, for the AFM case with $\gamma = -0.05$, appropriate for Fe$_4$. [4]

Finally, in Fig. 5 we show low-T plots at $N = 4$ of $\delta\tilde{\mathcal{C}}_{11}(\omega)$ versus $\omega|\alpha|^{1/2}/|J_1|$ for the special points $\gamma = \pm 1/3$, corresponding to the onsets of the central peak of the mode Ω_2. In both cases, curves for $|\alpha| = 160, 1280$ are shown. Remarkably, the FM and AFM cases are nearly identical, when plotted in this manner. As for the similar scalings at the endpoints of the the parameter range of the central peak for the isosceles triangle, [8] this scaling only applies to the frequency, without a corresponding scaling of $\delta\tilde{\mathcal{C}}_{11}(\omega)$, so that the overall scaling does not correspond to a scaling of the time in $\delta\mathcal{C}_{11}(t)$. However, for the isosceles triangle, the FM and AFM cases appeared to be nearly similar at temperatures that differed by a factor of about 8, whereas for the squashed tetrahedron, the temperatures are essentially identical.

VI. CONCLUSIONS

We have solved for the time correlation functions of the N-spin squashed equivalent neighbor model, with one spin coupled via the classical Heisenberg exchange J_1 to the $M = N - 1$ other spins, all of which are coupled to each other via a different Heisenberg exchange J_2. Our results are qualitatively similar to those of the isosceles triangle, $N = 3$, but show that for arbitrary $N \geq 3$, there are only four low-temperature modes, given by Eqs. (31)-(34) and (35)-(38) for ferromagnetic and antiferromagnetic signs of J_1, respectively.

At infinite T, we showed explicitly that the long-time asymptotic behavior of the autocorrelation function $\mathcal{C}_{11}^{\gamma=0}(t)$ on a prong of an M-pronged star approaches its asymtotic limit as $(t^*)^{-1}$. We also showed that for $3 \leq N \leq 8$, the infinite-T, long-time asymptotic limit

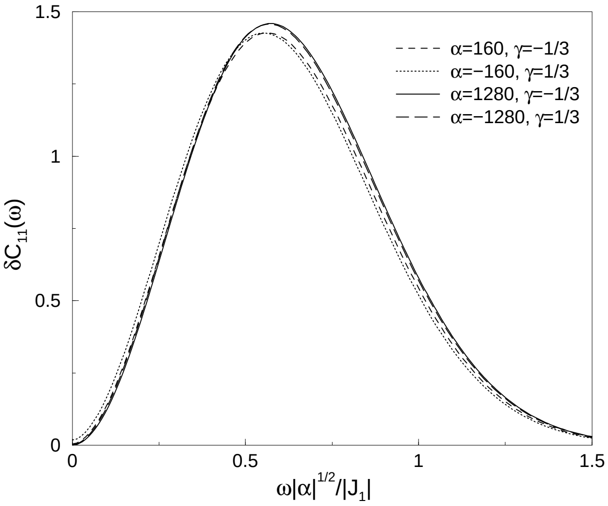

FIG. 5: Plots for $M = 3$ of $\delta\tilde{\mathcal{C}}_{11}(\omega)$ versus $\omega|\alpha|^{1/2}/|J_1|$ at $|\alpha| = 160, 1280$ for the Ω_2 modes at the onsets of the central peak, $\gamma = \pm 1/3$ for the FM and AFM cases, respectively.

of $\mathcal{C}_{NN}(t)$ is greater than that of $\mathcal{C}_{11}^{\gamma\neq 1}(t)$, and speculate that this relation is likely to hold for arbitrary N. We also showed that at infinite T, $\mathcal{C}_{11}^{0\neq\gamma\neq 1}(t)$ approaches its long-time asymptotic limit as $(\overline{t})^{-M}$, one power slower than does $\mathcal{C}_{NN}(t)$.

We showed explicitly that these mode frequencies apply for the isosceles triangle ($N = 3$) and for the squashed tetrahedron ($N = 4$). [8] For the particular parameter values appropriate for the single molecule magnet Fe$_4$, with four $S = 5/2$ Fe^{+3} spins on the corners of a squashed tetrahedron, we expect that this classical calculation of the Fourier transform of the time correlation functions will represent a reasonably good envelope of the δ-functions present in the quantum mechanical treatment of this model, provided that the temperatures are not too low with respect to $|J_1|$. Thus, we expect the qualitative features shown in Fig. 4 and the lower panel of Fig. 3 to be observable in inelastic neutron scattering studies of single crystals of Fe$_4$.

APPENDIX

The integrals appearing for $M \geq 3$ in Eq. (18) are

$$I_0 = \langle S_{1z0}^2 \rangle, \tag{A39}$$

$$I_1(t) = \langle \frac{A_N^2 S_{1z0}^2}{C_{1\to M}^2} \cos(st^*) \rangle, \tag{A40}$$

$$I_2(t) = \frac{1}{2} \langle (\Delta S_{1z0})^2 \cos[(1-\gamma)xt^*] \rangle, \tag{A41}$$

$$\begin{aligned} I_3(t) &= \frac{1}{4} \langle A_N^2 (\Delta S_{1z0})^2 \Big(\frac{\cos\{[s + (1-\gamma)x]t^*\}}{(x + C_{1\to M})^2} \\ &\quad + \frac{\cos\{[s - (1-\gamma)x]t^*\}}{(x - C_{1\to M})^2} \Big) \rangle. \end{aligned} \tag{A42}$$

The density of states for N spins is given by [10]

$$\begin{aligned} \mathcal{D}_N(x) &= \Theta(x) \sum_{p=0}^{E[(N-1)/2]} \Theta(N - 2p - x) \\ &\quad \times \Theta(x - N + 2p + 2) d_{N-2p}(x), \end{aligned} \tag{A43}$$

$$d_{N-2p}(x) = \sum_{k=0}^{p} \frac{(-1)^k (N - 2k - x)^{N-2}}{2^{N-1}(N-2)!} \binom{N}{k}, \tag{A44}$$

where $E(x)$ is the largest integer in x and $\Theta(x)$ is the Heaviside step function. As noted in Eq. (13), the $I_i(t)$ contain integrations over $\mathcal{D}_{M-1}(y)$.

Although the $I_i(t)$ are explicitly triple integrals over x, y, and s, the only y dependence of the integrand appears in the expressions for S_{1z0}^2 and $(\Delta S_{1z0})^2$, given by Eqs. (11) and (12) plus the expressions following Eq. (7). In most of these integrals, one has to evaluate

$$I_i = \int_0^{M-1} dy \int_{|y-1|}^{y+1} dx g_M(x, y) f(x, t) \tag{A45}$$

$$\begin{aligned} &= \int_0^{M-2} dx f(x, t) \int_{|x-1|}^{x+1} dy g_M(x, y) \\ &\quad + \int_{M-2}^{M} dx f(x, t) \int_{|x-1|}^{M-1} dy g_M(x, y), \end{aligned} \tag{A46}$$

where $g_M(x, y)$ has either the form $a(x)[1 - (x^2 + 1 - y^2)^2/(4x^2)]\mathcal{D}_{M-1}(y)$ or the form $a(x)(x^2 + 1 - y^2)^2 \mathcal{D}_{M-1}(y)$, and $f(x, t)$ involves an integral over s. In most cases, the y integrals can be performed before the x integrals, reducing the triple integrals to double integrals, precisely as was done for the equivalent neighbor model with $M \to N$.[10]

We now calculate the exact infinite-time, infinite-temperature limit of the correlation function $\mathcal{C}_{11}(t)$ for $\gamma \neq 1$ from Eq. (A39). We first perform the integration over s, and then invert the order of the remaining two integrations, as outlined above. For $N = 4$, we then find,

$$\begin{aligned} \lim_{\substack{t\to\infty \\ T\to\infty}} \mathcal{C}_{11}^{\gamma\neq 1}(t) &= \frac{29}{360} + \frac{\pi^2}{384} + \frac{83}{360}\ln 2 + \frac{3}{40}\ln 3 \\ &\quad - \frac{1}{96}\left[\mathrm{Li}_2\left(-\frac{1}{2}\right) + \mathrm{Li}_2\left(-\frac{1}{3}\right)\right] \\ &\quad - \frac{1}{192}\left[\ln\left(\frac{2}{3}\right)\right]^2 \\ &\approx 0.355496, \end{aligned} \tag{A47}$$

where $\mathrm{Li}_2(z)$ is the standard dilogarithm function,

$$\mathrm{Li}_2(z) = \int_z^0 \frac{\ln(1-t)}{t} dt. \tag{A48}$$

The exact formulae become increasingly complicated with increasing N, so in Table I, we only list the numerical values of those additional ones for $3 \leq N \leq 11$, along with those of the infinite t, T limits of $\mathcal{C}_{NN}(t)$.

N	$\lim_{\substack{t\to\infty\\ T\to\infty}} \mathcal{C}_{11}^{\gamma\neq 1}(t)$	$\lim_{\substack{t\to\infty\\ T\to\infty}} \mathcal{C}_{NN}(t)$
3	0.370130	0.480521
4	0.355496	0.436345
5	0.342702	0.416362
6	0.337024	0.401888
7	0.333611	0.384419
8	0.331595	0.378635
9	0.330327	0.374027
10	0.329516	0.370270
11	0.328992	0.367148

TABLE I: Infinite t, T limits of the autocorrelation functions

Next, we sketch our procedure for obtaining $\lim_{T\to\infty} \delta\mathcal{C}_{11}^{0\neq\gamma\neq 1}(t)$ as $\overline{t} \gg 1$ for arbitrary N. From Eq. (A41), we first perform the integration over s, giving us a function proportional to $f(x)$ given by Eq. (25). To avoid the singularity at $x = 1$, we do not invert the order of the remaining two integrals, but instead integrate with respect to x by parts twice, leading to

$$\lim_{\substack{T\to\infty\\ \overline{t}\gg 1}} \delta\mathcal{C}_{11}^{\gamma\neq 0,1}(t) \sim -\frac{1}{8\overline{t}^2}\sum_{\sigma=\pm 1}\int_0^{M-1} y dy \mathcal{D}_{M-1}(y) \times f(y+\sigma)\cos[(y+\sigma)\overline{t}]. \tag{A49}$$

We then integrate with respect to y a total of $M-2$ times, noting that all terms proportional to derivatives of f sum to zero. We finally obtain,

$$\lim_{\substack{T\to\infty\\ \overline{t}\gg 1}} \delta\mathcal{C}_{11}^{\gamma\neq 0,1}(t) \sim \frac{1}{(\overline{t})^M}\sum_{p=0}^{\mathrm{E}(M/2)} A_{Mp} f(M-2p) \times\cos[(M-2p)\overline{t} + M\pi/2], \tag{A50}$$

$$A_{Mp} = \frac{(-1)^{p+M}}{2^{M+1}}\Big[(1-\delta_{p,M/2}) \times(M-2p-1)\binom{M-1}{p} -(1-\delta_{p,0})(M-2p+1) \times\binom{M-1}{p-1}\Big], \tag{A51}$$

where $f(x)$ is given by Eq. (25). We note that $f(0) = \frac{8}{3}$ and $f(1) = 2$.

We now sketch our derivations of the low-temperature mode frequencies. We first note from Eqs. (17) and (A40) that the Fourier transforms of $\delta\mathcal{C}_{NN}(t)$ and $I_1(t)$ both contain $\delta(s-\tilde{\omega})$, where $\tilde{\omega} = \omega/|J_1|$. From the above discussion, each of these then can be reduced to a single integral over x,

$$K_0(\tilde{\omega}) = \int_{|\tilde{\omega}-1|}^{\min(\mathrm{M},\tilde{\omega}+1)} dx Q_N(x,\tilde{\omega}) e^{[\alpha(\gamma-1)x^2+\tilde{\omega}^2]}, \tag{A52}$$

where $Q_N(x,\tilde{\omega})$ is different for $\delta\tilde{\mathcal{C}}_{NN}(\omega)$ and the Ω_1 mode contribution to $\delta\tilde{\mathcal{C}}_{11}(\omega)$. In both cases it is independent of α and T, and is therefore irrelevant to the determination of the mode frequency Ω_1 in the limit $T \to 0$. The integration limits arise from the condition that the δ-function is restricted by $|x-1| \leq s \leq x+1$. For the FM case, $\alpha > 0$, we first consider the case $\gamma < 0$. As $\alpha \to \infty$, the integral is maximized by choosing x to have its minimum value, $x = |\tilde{\omega}-1|$. We then maximize the resulting expression for the exponent as a function of $\tilde{\omega}$, which occurs at $\tilde{\omega} = \tilde{\omega}^* = 1 - 1/\gamma$. For $\gamma > 1$, the minimum x value, $|\tilde{\omega}-1|$, is limited for large $\tilde{\omega}$ by M, so $\tilde{\omega}^* = N$. The crossover occurs when these frequencies are equal, $N = 1-1/\gamma$, or $\gamma = -1/M$. Setting $\tilde{\omega}^* = \Omega_1/|J_1|$, we thus recover Eq. (31). For the AFM case as $T \to 0$, $\alpha \to -\infty$, we want to minimize $(\gamma-1)x^2 + \tilde{\omega}^2$ in the exponent. For $\gamma > 1$, this occurs at $x = |\tilde{\omega}-1|$, and for $\gamma < 1$, it occurs at $x = \tilde{\omega}+1$. In both cases, optimizing the exponent leads to $\tilde{\omega}^* = |1-1/\gamma|$. The latter case is restricted by the limitation $\tilde{\omega}^* = M-1$. The crossover between these two limits occurs at $M = |1-1/\gamma|$, or $\gamma = 1/M$. Setting $\tilde{\omega}^* = \Omega_1/|J_1|$, we then recover Eq. (35).

We now focus on the integral $I_2(t)$, Eq. (A41). We first perform the y integral as sketched above. Then, the integral over s does not contain any time dependence, and as $T \to 0$, it is dominated by the factor $\exp(\alpha s^2)$. After integration by parts, we obtain the single integral over x, which has the form

$$I_2(t) \sim \int_0^M dx P_N(x)\exp[\alpha(\gamma x^2 \pm 2x)]\cos[(1-\gamma)xt^*], \tag{A53}$$

where $P_N(x)$ is independent of α, as in Eq. (4). Fourier transformation then involves the δ-function, $\delta(\tilde{\omega} - |1-\gamma|x)$, so that the position of the mode due to I_2 is found by optimizing the expression $\exp\{\alpha[\gamma\tilde{\omega}^2/(1-\gamma)^2 \pm 2\tilde{\omega}/|1-\gamma|]\}$. For the FM case and $\gamma < 0$, we maximize this function with the + sign, leading to $\tilde{\omega}^* = 1-1/\gamma$. For $\gamma > 0$, the δ-function was restricted by $x \leq M$, leading to $\tilde{\omega}^* = M|1-\gamma|$. These values for $\Omega_3/|J_1| = \tilde{\omega}^*$ are equal at $\gamma = -1/M$. Combining, we obtain the FM Ω_3 mode frequencies, Eq. (33). For the AFM case as $\alpha \to -\infty$, we choose the $-$ sign in the above exponent, and minimize $\gamma\tilde{\omega}^2/(1-\gamma)^2 - 2\tilde{\omega}$ in the exponent. For $\gamma > 0$, this occurs at $\tilde{\omega}^* = |1-1/\gamma|$. For $\gamma < 0$, the overall exponent is bounded by $\tilde{\omega}^*/|1-\gamma| \leq M$. Combining, we obtain the expressions for $\Omega_3/|J_1|$ for the AFM case, Eq. (37).

We now turn our attention to I_3. In taking the Fourier transform, there are four δ-functions, $\delta[\tilde{\omega}-s-(1-\gamma)x]$, $\delta[\tilde{\omega}+s+(1-\gamma)x]$, $\delta[\tilde{\omega}+s-(1-\gamma)x]$, and $\delta[\tilde{\omega}-s+(1-\gamma)x]$. These δ-functions lead after the usual reductions of the y integrals to the following integrals, respectively,

$$K_1(\omega) = \int_{\max[(1-\tilde{\omega})/\gamma,(\tilde{\omega}-1)/(2-\gamma)]}^{\min[M,(\tilde{\omega}+1)/(2-\gamma)]} dx R_{N1}(x,\tilde{\omega})$$

$$\times f_+(x,\tilde{\omega}), \qquad \text{(A54)}$$

$$K_2(\omega) = \Theta(\gamma-1)\int_{\max[0,(1+\tilde{\omega})/\gamma,(\tilde{\omega}-1)/(\gamma-2)]}^{\min[M,\Theta(\gamma-2)(\tilde{\omega}+1)/(\gamma-2)]} dx$$

$$\times R_{N2}(x,\tilde{\omega}) f_-(x,\tilde{\omega}), \qquad \text{(A55)}$$

$$K_3(\omega) = \Theta(1-\gamma)\int_{\max[0,-(1+\tilde{\omega})/\gamma,(\tilde{\omega}+1)/(2-\gamma)]}^{\min[M,(1-\tilde{\omega})/\gamma]} dx$$

$$\times R_{N3}(x,\tilde{\omega}) f_+(x,\tilde{\omega}), \qquad \text{(A56)}$$

$$K_4(\omega) = \int_{\max[0,(\tilde{\omega}-1)/\gamma]}^{\min[M,(\tilde{\omega}+1)/\gamma]} dx$$

$$\times R_{N4}(x,\tilde{\omega}) f_-(x,\tilde{\omega}), \qquad \text{(A57)}$$

$$f_\pm(x,\tilde{\omega}) = \exp\{\alpha[\tilde{\omega}^2 + \gamma(\gamma-1)x^2 \pm 2\tilde{\omega}(\gamma-1)x]\}, \qquad \text{(A58)}$$

where the $R_{Ni}(x,\tilde{\omega})$ are independent of T.

We first consider the AFM case of K_1, $\alpha \to -\infty$. For $\gamma > 1$, all terms in the exponent are negative, so we need to minimize the function $\tilde{\omega}^2 + \gamma(\gamma-1)x^2 + 2x\tilde{\omega}(\gamma-1)$. Setting $x = (\tilde{\omega}-1)/(2-\gamma)$, and optimizing this function with respect to $\tilde{\omega}$, we find that its minimum occurs at $\tilde{\omega}^* = 2(1-1/\gamma)$. For $\gamma < 0$, the last term in the function to be minimized is negative, so we take $x = (\tilde{\omega}+1)/(2-\gamma)$ from the upper integration limit. Optimizing the function, we find $\tilde{\omega}^* = 2(1/\gamma - 1)$, so both γ regions satisfy $\tilde{\omega}^* = 2|1-1/\gamma|$. However, this is subject to the constraint on the upper integration cutoff, which is $(\tilde{\omega}^*+1)/(2-\gamma) = M$, or $\tilde{\omega}^* = 2M - 1 - M\gamma$. These values are equal at $\gamma = 1/M$. Altogether, $\tilde{\omega}^* = \Omega_4/|J_1|$ for the AFM case in Eq. (38). For the FM case with $\gamma < 0$, we take $x = (\tilde{\omega}+1)/(2-\gamma)$, optimize, and again obtain $\tilde{\omega}^* = 2(1-1/\gamma)$. The cutoff occurs when the lower limit, $x = (\tilde{\omega}-1)/(2-\gamma)$, equals M, giving $\tilde{\omega}^* = 2M + 1 - M\gamma$. The crossover occurs at $\gamma = 1/M$, as given by Eq. (34) for $\Omega_4/|J_1|$.

Next, we consider the FM case of K_4. First for $\alpha \to \infty$, $\gamma < 0$, it is easily seen that the exponent in $f_-(x\tilde{\omega})$ is positive definite. Thus, we might expect the upper limit for x to apply. But, this is either the cutoff, M, or a negative quantity, $(\tilde{\omega}+1)/\gamma$. Thus, the only positive limit is the lower cutoff, $x = (\tilde{\omega}-1)/\gamma$, which can be positive for $\tilde{\omega} < 1$, leading to a larger exponent than obtained by setting $x = 0$. However, $f_-[(\tilde{\omega}-1)/\gamma, \tilde{\omega}] = \exp[(\alpha/\gamma)(\tilde{\omega}^2 + \gamma - 1)]$, which for $\alpha > 0$, $\gamma < 0$ has a maximum at $\tilde{\omega}^* = 0$, corresponding to a central peak. This will be the mode frequency until $(\tilde{\omega}-1)/\gamma = M$, the upper cutoff, resulting in $\tilde{\omega}^* = 1 + M\gamma$. The crossover occurs at $\gamma = -1/M$. Thus, this mode reduces to $\Omega_2/|J_1|$ as given by Eq. (32). For the AFM case for $\gamma > 0$, we set $x = (\omega+1)/\gamma$, and again we find $f_-[(\tilde{\omega}+1)/\gamma, \tilde{\omega}] = \exp[-(|\alpha|/\gamma)(\tilde{\omega}^2 + \gamma - 1)]$, which has a maximum at $\tilde{\omega}^* = 0$. This form continues until $(1-\tilde{\omega})/\gamma = M$, which occurs at $\tilde{\omega}^* = 1 - M\gamma$. The crossover occurs at $\gamma = 1/M$. Thus, this gives rise to the mode $\Omega_2/|J_1|$ in Eq. (36).

We now consider the K_2 integral. This makes a very small contribution, because of the the severe limitation that it vanishes unless $\gamma > 1$. For the AFM case, the exponent is optimized at $x = x^* = \tilde{\omega}/\gamma$, and then optimizing the mode frequency with respect to $\tilde{\omega}$, we find that $\tilde{\omega}^* = 0$, so that K_2 for AFM coupling contributes to $\Omega_2/|J_1|$. For the FM case, the maximum exponent occurs at $x = M$, and from the δ-function restrictions, we see that K_2 makes a contribution to the $\Omega_4/|J_1|$ mode.

Finally, we discuss briefly the K_3 case, for which $\gamma < 1$. Setting $\gamma < 0$ for the FM case, the optimum situation is obtained when $\tilde{\omega}^* = 0$, so that it adds to the $\Omega_2/|J_1|$ mode. For the AFM case, the optimum x value is $x^* = -\tilde{\omega}/\gamma$, and this is restricted by $x \leq M$. Hence, K_3 essentially makes a contribution to the Ω_2 mode for the AMF case, as well.

---

[*] Electronic address: ma22@cornell.edu
[†] Electronic address: rklemm@mpipks-dresden.mpg.de

[1] A. Cornia, R. Sessoli, L. Sorace, D. Gatteschi, A. L. Barra, and C. Daiguebonne, Phys. Rev. Lett. **89**, 25701 (2002).
[2] A. Bino, D.C. Johnston, D.P. Goshorn, T.R. Talbert, and E.I. Stiefel, Science **241**, 1479 (1988).
[3] Y. Furukawa, M. Luban, R. Borsa, D.C. Johnston, A.V. Mahajan, L.L. Miller, D. Mentrup, J. Schnack, and A. Bino, Phys. Rev. B **61**, 8635 (2000).
[4] A. L. Barra, A. Caneschi, A. Cornia, A. Fabrizi de Biani, D. Gatteschi, C. Sangregorio, R. Sessoli, and L. Sorace, J. Am. Chem. Soc. **121**, 5302 (1999).
[5] A. Bouwen, A. Caneschi, D. Gatteschi, E. Goovaerts, D. Schoemaker, L. Sorace, and M. Stefan, J. Phys. Chem. **105**, 2658 (2001).
[6] D. Mentrup, J. Schnack, and M. Luban, Physica A **272**, 153 (1999).
[7] D. Mentrup, H. J. Schmidt, J. Schnack, and M. Luban, Physica A **278**, 214 (2000).
[8] M. Ameduri and R.A. Klemm, Phys. Rev. B **66**, 224404 (2002) (cond-mat/0108213).
[9] R.A. Klemm and M. Luban, Phys. Rev. B **64**, 104424 (2001).
[10] R.A. Klemm and M. Ameduri, Phys. Rev. B **66**, 012403 (2002).
[11] D.V. Efremov and R.A. Klemm, Phys. Rev. B **66**, 177427 (2002).
[12] O. Ciftja, Physica A **286**, 541 (2000).
[13] E.T. Whittaker and G.N. Watson, *A Course of Modern Analysis* (Cambridge University Press, Cambridge, 1999) p 172.